Pseudo-elastic Flexure-Hinges in Robots for Micro Assembly

Jürgen Hesselbach and Annika Raatz*

Institute of Machine Tools and Production Technology
Technical University Braunschweig, Germany

ABSTRACT

The increasing tendency of products towards miniaturization makes the substitution of conventional hinges to flexure hinges necessary, since they can be manufactured almost arbitrarily small. On account of their multiple advantages like no backlash, no slip-stick-effects and no friction, their application is especially reasonable in high-precision robots for micro assembly.
Particular pseudo-elastic shape memory alloys offer themselves as material for flexure hinges. Since flexible joints gain their mobility exclusively via the elastic deformation of matter, the attainable angle of rotation is strongly limited when using conventional metallic materials with approximately 0.4% maximal elastic strain. Using pseudo-elastic materials, with up to 15% elastic strain, this serious disadvantage of flexure hinges can be avoided.
A further problem of flexible joints is their kinematic behavior since they do not behave exactly like conventional rotational joints. In order to examine the kinematics of the hinges an experimental set-up was developed whereby good compliance with theoretical computed values could be achieved. A three (+1) degree of freedom parallel robot with integrated flexure hinges is investigated showing its kinematic deviations to its rigid body model. The data of the kinematic model of the flexible joint can then be implemented into the control of this compliant mechanism in order to gain not only a higher repeatability but also a good absolute accuracy over the entire working space.

Keywords: flexible hinges, pseudo-elastic SMA, high precision robotics, kinematic behavior, compliant mechanism, instantaneous center of rotation

1. INTRODUCTION

More and more micromechanical products are built in place of micro-systems, due to functional and economical reasons. That means the products will combine actors, sensors and signal processing on smallest room. These products are often built in hybrid technology, which means that they are made of different parts so that some kind of assembly is required. Until today micro-systems are often manufactured by hand. Unfortunately, this leads to high human (labor) demands under different circumstances making it's use exclusive to single and small series productions. To achieve economic efficiency, an automatic production system needs to be in place in order to produce higher # of items at a consistent quality level.

One possible solution is the development of robots based on closed kinematic chains, called parallel-structures, with dimensions far smaller than conventional robots for industrial use. Due to the fact that the actuators of parallel-robots are fixed to the frame and do not have to be moved, a very light and stiff structure can be realized. This leads to high dynamics and high positioning accuracy, with less constructive and economic effort in comparison to conventional serial robots.
Especially simple is the integration of flexure hinges in parallel-structures, because all joints are passive. Due to the natural lack of backlash, friction and slip-stick-effects in flexure hinges, the accuracy of positioning can be highly increased and parallel robots with flexure hinges are even extremely suitable for assembly-tasks under clean room conditions
Because of the physics of scaling, non-linear surface forces are more important in micro-structures and not the inertial forces which influences the dynamics in conventional scale structures. So these advantages of flexure hinges make the difference especially beneficial for small scale devices. Therefore, flexure joints are also used in numerous applications.[1,2,3].

1.1. Flexure Hinges

Flexure hinges gain their mobility from an elastic and plastic deformation exclusively. To achieve a high life cycle the deformation should remain in the elastic strain. Looking at a conventional flexure hinge, a cantilever beam with a circular

* Correspondence: Email: a.raatz@tu-bs.de; http://www.iwf.ing.tu-bs.de; Langer Kamp 19b, 38106 Braunschweig

Microrobotics and Microassembly II, Bradley J. Nelson, Jean-Marc Breguet, Editors,
Proceedings of SPIE Vol. 4194 (2000) © 2000 SPIE · 0277-786X/00/$15.00

notch (fig. 1) (further referred as notch hinge), the deformation takes place nearly only at the point of the smallest cross-section. Flexure hinges made of metallic alloys used for springs have limited mobility because these materials only allow low elastic strains. Hinges made of these materials are mostly used in precision engineering e.g. in bearings for highly accurate measuring instruments. These hinges have the geometry of leaf springs which allow deformation over the whole hinge length. Therefore, the possible deflections are higher and can be suited to the needs by varying the length.
One possibility is the use of plastics for notch hinges, due to their higher elastic strains. Especially thermoplastics as polyacetalresin (POM) offer themselves, which show high strength and stiffness. It also offers a good resilient behavior and a good cutting machinability. Flexure hinges made of plastics are used in various one-way products, e.g. in snap hinge closure, because they allow cheap mass production by injection molding.

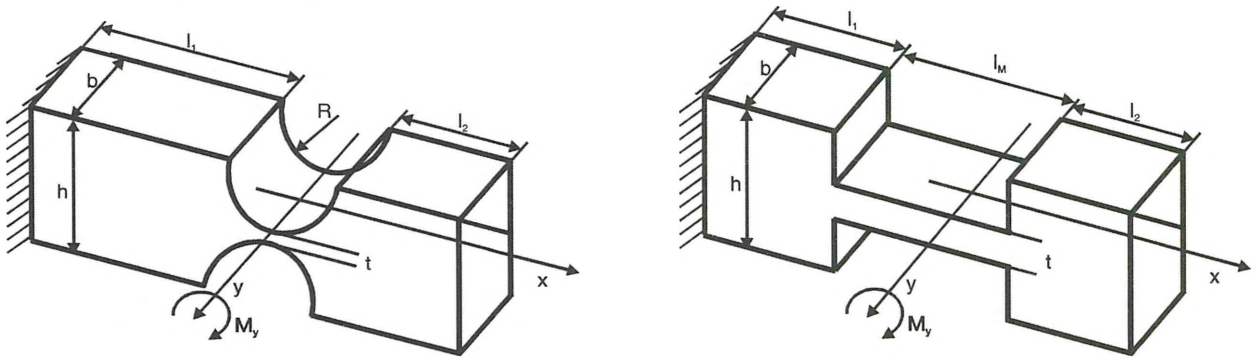

Figure 1. Diagram of a typical notch flexure hinge (left) and a flexure hinge similar to a leaf spring (further referred as beam hinge)
y is the nominal axis of rotation

Paros and Weisbord developed an analytic solution for the determination of the angular compliance of notch hinges under various forces and moments.[4] By taking the geometrical moment of inertia and under the consumption of linear elastic material behavior, the maximum angular deflection of a flexure notch hinge can be developed

$$\phi_{B,\max} = \frac{3\pi\sigma_{\max} R^{1/2}}{4Et^{1/2}}. \qquad (1)$$

The permitted angular deflection of a hinge made of POM with the dimensions (R=5 mm, t=0.1 mm) and the modulus of elasticity E = 3000 N/mm², $\sigma_{bw,\max}$ = 30 N/mm² is determined to $\phi_{B,\max} = 9.8°$. The main disadvantage of plastics is their tendency to creep at room temperature. This disadvantage can be equalized by the use of pseudo-elastic shape memory alloys (SMA) which also show high reversible range of strain, but do not show the tendency to creep like plastics. Horie et al. have already used pseudo-elastic leaf springs in a pantograph-mechanism.[5] Especially in structures which are prestressed in order to reach a higher positioning accuracy the use of SMA should be preferred.

1.2. Pseudo-elastic material behavior of SMA

Depending on the temperature or the loads, shape memory alloys exist in at least two different phases: the high-temperature phase austenite and the low temperature phase martensite. The martensitic phase transformation is diffusionless and the transformation of the austenitic lattice to the martensitic one is determined by shearing processes. In order to receive a reversibility for many cycles there should arise only a few nonreversible lattice defects during transformation. A description of the main correlation and properties of SMA follows for the simple case of uniaxial tensile stress (fig. 2).[6]

At temperatures lower than M_F SMA are in an unoriented twinned martensitic phase (fig. 2a). If the test specimen is deformed by an external tension, it behaves linear-elastically with small strain rates. Upon arriving at a so-called pseudo yield stress the martensite is detwinned and the sample is apparently plastically deformed. Having passed the pseudoplastic strains (martensite plateau, characterized by a constant stress), the sample further deforms elastically and then as a conventional material. That is, upon arriving at yield stress R_p it behaves plastically with displacement formation and movement up to failure. Heating the sample after a pseudoplastic deformation to a temperature A_F, the material is

transformed into its high temperature phase austenite. In this process the sample's original shape is recovered completely and the pseudoplastic strains disappear. Cooling the specimen to a temperature M_F the reverse transformation from austenite to martensite occurs, but this transformation is normally no subject to any deformation. This thermal characteristics of SMA are used in the application as an actuator with an external restoring force.

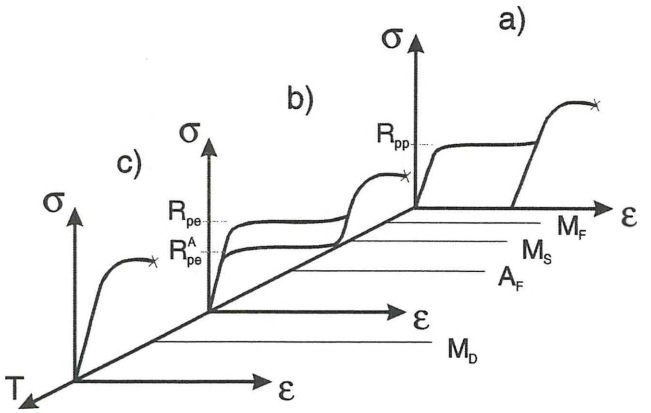

Figure 2. Stress-strain-diagram of shape memory alloys at different temperatures

In the temperature interval A_F to M_D the material is in its austenitic phase (fig. 2b). Upon loading the sample initially deforms elastically. Arriving at the plateau stress R_{pe} a stress-induced conversion of austenite into martensite begins, resulting in high pseudo-elastic strain rates at nearly constant stresses. This is because of the formation of untwinned martensite of the austenite. At the end of the stress plateau the sample is completely martensitic. During a subsequent release below a limiting stress R_{pe}^A a reverse transformation from martensite to austenite occurs. This is a result of the instability of the martensite at lower stresses, thus making the stress-strain path a closed hysteresis loop. Because of the reversible strains the sample is fully recovered to its undeformed shape. Additional loading passing the upper stress plateau causes an at first elastic and subsequently plastic, nonreversible deformation up to failure.
The high strain intervals at nearly constant stress can be used in many applications where in comparison great displacements must be set up at unchangeable forces. Depending on the chemical composition and the thermo-mechanical treatment SMA on the basis of NiTi have recoverable strain rates up to 8%. Because of its good biocompatibility NiTi alloys are often used in medical applications as stents, minimal invasive surgery instruments or orthodontic wires.
For temperatures above M_D no stress-induced martensite can be formed (fig. 2c). The austenitic test specimen shows conventional material behavior with elastic and plastic deformation up to failure. Consequently the pseudo-elastic material behavior of SMA is limited to a certain temperature range M_S-M_D. For use in flexure hinges in handling devices the temperature range must be around room temperature, performed via a suitable production and chemical composition.
Single crystals of the CuZnAl or CuAlNi alloys also show pseudo-elastic behavior. These materials can achieve reversible strain rates up to 15% and more. Stress-strain-diagram of a CuAlNi single crystal uniaxial tensile tests are different having two pseudo-elastic stress plateaus. But the stress plateaus are based both on the formation of stress-induced martensite.

It's not possible to determine the maximal angle deflection of a pseudo-elastic flexure hinge via the analytic expression from Paros and Weisbord, because Eq. 1 only applies for linear elastic behavior. Instead of the angle can be computed with a FEM program, e.g. ANSYS. Since several approaches for modeling the pseudo-elastic behavior exist but none is implemented in the program ANSYS, the material behavior was alternatively described with the material model MELAS.[7] At this multi linear elastic material model, the loading path of the stress-strain-curve can be copied via the input of single stress-strain points, e.g. achieved by a tensile test. Because the unloading runs back the same path, the hysteresis cannot be modeled. However, this is not necessary for the definition of a maximum angle of deflection.
For a flexure hinge with the identical dimensions as the above described made by POM you get a maximum angle of bending up to $\phi_{B,max} = 20°$ for pseudo-elastic material. A verification of the joint angle was made for the material POM as well. An angle of 9.6° was determined, the same as computed analytically. Therefore by the use of pseudo-elastic material twice as great angles of deflection can be achieved.

In order to be able to successfully integrate flexure hinges in parallel robots, the special kinematic behavior of flexure hinges has to be considered. A flexure hinge does not behave itself as an ideal conventional joint, with a fix point of

rotation. Rather, the point of rotation of a flexure hinge moves depending on the geometrical dimensions and the bending angle. For small angles and small hinge lengths, this movement may be negligible, but not for greater angles. In figure 3 the displacements of point B of a flexure hinge and of an ideal rotational joint are represented. The resulting deviations are $\Delta r = 80\ \mu m$ at an angle of $\phi_B = 20°$.

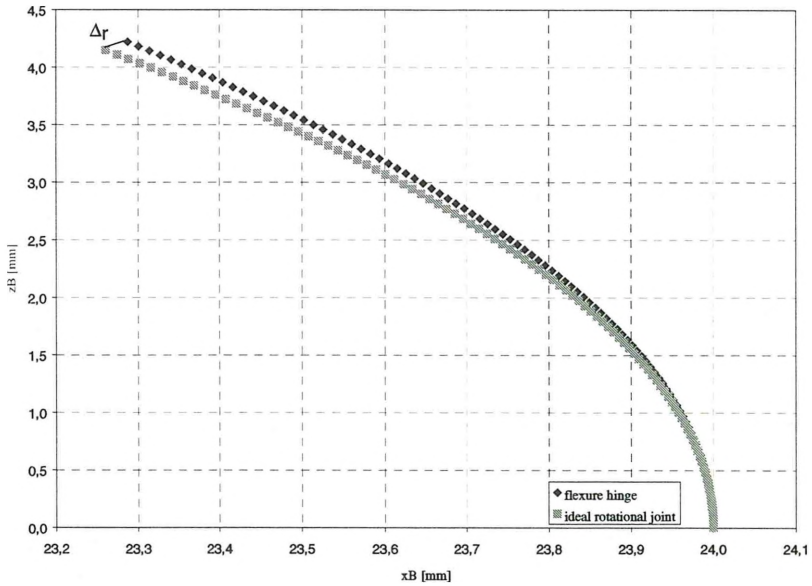

Figure 3. Deflection curves of a flexure hinge and an ideal conventional joint, showing the deviations Δr at angles from 0° to 20°

2. KINEMATIC DESCRIPTION OF FLEXURE HINGES

To derive a kinematic description of flexure hinges the deflection curve of a point lying on hinge link 2 (l_2) has to be determined. The hinge is cantilevered at $x = 0$ and forces or moments are exerted in point B. The displacement curve of point B is characterized by the coordinates x_B, z_B and ϕ_B at different loads. Assuming link 2 to be rigid, the angles ϕ_C and ϕ_B are identical and ϕ_B corresponds to the hinge angle (fig. 4).

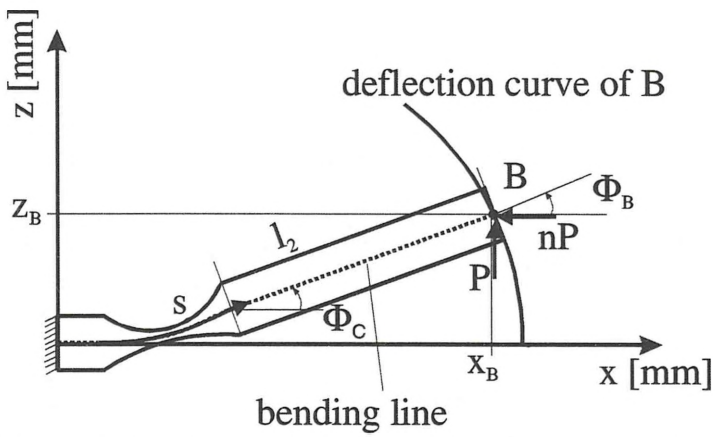

Figure 4. Bending line and deflection curve characterized by (x_B, z_B, ϕ_B) of a flexure hinge

For the determination of the coordinates of point B the deflection curve bending line of the hinge must be calculated. Assuming the geometrical moment of inertia to be a function of the beam length s, the bending line of a cantilever beam can be computed as well.[8]

With the assumption that the material is linear elastic, the undeflected beam axis is straight, the plane of symmetry is identical with the loading plane are, the cross sections remain even and the beam length is large to the cross-sectional dimensions, the following well-known beam moment-curvature differential equation system can be deduced:
(s- beam length of curve, x- coordinate along the undeflected beam axis, z- transverse deflection, ϕ- angular deflection of the beam axis with the x-axis, M- moment, E- Young-Modulus, I- geometrical moment of inertia, $d\phi/ds=1/R$- curvature)

$$\frac{d\phi_M}{ds} = \frac{M(s)}{EI(s)} \tag{2}$$

$$\frac{dx}{ds} = \cos\phi \tag{3}$$

$$\frac{dz}{ds} = \sin\phi \tag{4}$$

Loading a flexure hinge it must be assumed that the beam length is not long in comparison to the cross sectional dimensions. Therefore, in addition to the deflection due to a moment, the influence of the transverse force Q also has to be considered.
With the shear stress $\tau = \mu Q/A$ along the neutral surface A and the modulus of shear G an additional curvature occurs because of the shear stress

$$\frac{d\phi_Q}{ds} = \frac{\mu}{A^2 G}\left(\frac{dQ}{ds}A - Q\frac{dA}{ds}\right), \tag{5}$$

where μ is a factor, which depends on the geometry of the cross section. Filonenko-Boroditsch calculates μ for a rectangular cross section to 6/5 by using the passive deformation work.[9]
In case of large deflections, the balance conditions necessary for the calculation of the bending moment must be set at the deformed beam / hinge.
Differential dependency of the internal force Q thereby deduces to:

$$\frac{dQ}{ds} = -\frac{MN}{EI} \tag{6}$$

To accomplish a general load-case a force P in z-direction and a force nP perpendicularly to it are set. Then the internal forces Q and N result to:

$$N(s) = P\sin\phi - nP\cos\phi, \tag{7}$$

$$Q(s) = P\cos\phi + nP\sin\phi, \tag{8}$$

and the moment is

$$M = P(x_B - x) + nP(z_B - z). \tag{9}$$

Adding the curvatures $d\phi_Q/ds$ (Eq. 5) due to the shear stress and the one due to the normal stress $d\phi_M/ds$ (Eq. 2) and using the relations from Eq. 6 to 8, with the moment M from Eq. 9, the following result for the total curvature deduces to:

$$\frac{d\phi}{ds} = \frac{M(s)}{EI(s)} + \frac{\mu}{A^2(s)G}\left(-\frac{M(s)A(s)}{EI(s)}\left(P\sin\phi + nP\cos\phi\right) - \left(P\cos\phi - nP\sin\phi\right)\frac{dA(s)}{ds}\right). \tag{10}$$

The differential equation system can then be solved, for example, using the Runge-Kutta method with an additional iteration over the coordinates of point B, used in Eq. 9. An external moment in Point B only has to be added to M in Eq. 9.

Actually, these equations apply only to linear elastic material behavior. However, a constitutive model by Prandtl-Reuss can be integrated easily, that quite well approximates the pseudo-elasticity.
If only the deflections are of interest and not the effecting loads and stresses the stress-strain relationship of the material has no influence. Also the factor n, thus a working tensile force or compressive force, and the transverse force Q do not have big influence to the deflection curves of notch flexure hinges from a certain length for l_2 up.[8,10]

Now if the deflection curve of one point of the flexure hinge is well-known during load, the movement of the center of rotation can be calculated. The movement of a body in a plane can always be described by an unreeling movement of a moving centroide on a fixed centroide (fig. 5).[11]

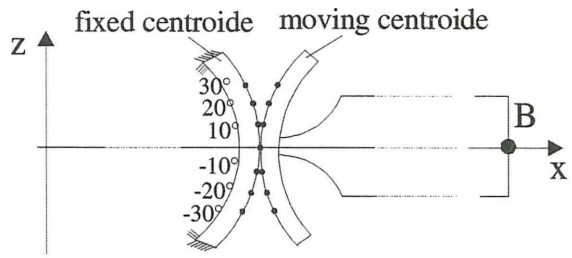

Figure 5. Kinematic model of a flexure hinge with unreeling centroides

The curve of the instantaneous centers of rotation can now be determined either graphically or computationally from the coordinates (x_B, z_B, ϕ_B) of the deflection curve. The coordinates of the instant centers at different joint angles are given by:

$$x_P = x_B - \frac{dy_B}{d\phi_B}, \tag{11}$$

$$z_P = y_B + \frac{dx_B}{d\phi_B}. \tag{12}$$

Because the coordinates of point B are determined discretely, x_P and z_P must be calculated over the difference quotient. A second possibility of calculating x_P and z_P is to derive functional dependencies $y_B = f(\phi_B)$ and $x_B = f(\phi_B)$ and afterwards form the differential quotient.

1.3. Experimental setup

For the examination of the analytically deduced deflection curve an experimental setup (fig. 6) was developed. The hinge is deflected with a four-bar linkage driven by a step motor. Loads affecting the hinge are measured with a 6-axis force-moment sensor. The sensor has a resolution of 0.0125 N for the forces and 0.0625 Nmm for the moments. A CCD-camera is integrated above the joint, which can record the movement of the joint.
The images are analyzed with the digital image processing tool OPC (optical position control) developed by the institute of Metrology and Experimental Mechanics, TU Braunschweig. For the measurement of the deflections of a point on the hinge in x and z direction and the rotation of the hinge two points are optically pursued. The measurements are derived on an area based algorithm. That is, not an individual image point is regarded, but rather an area with multiple pixels. The area is characterized over their specific intensity distributions. During the measurement of the deflection of the hinge, the intensity distributions of two related object states are compared to each other. The intensity distributions of these two related object states are fitted until the difference of the intensity distributions become minimal. The resulting shift is identical with the deflection of the hinge. Because all pixels of the area are containing information for correlation, the accuracy of determining the position is higher compared to feature based algorithms. A camera with 782x582 pixels is used and the measurement area was 15x11 mm² with a window size of 31x31 pixels. The resolution can then be expected to be 0.1 µm.[12]

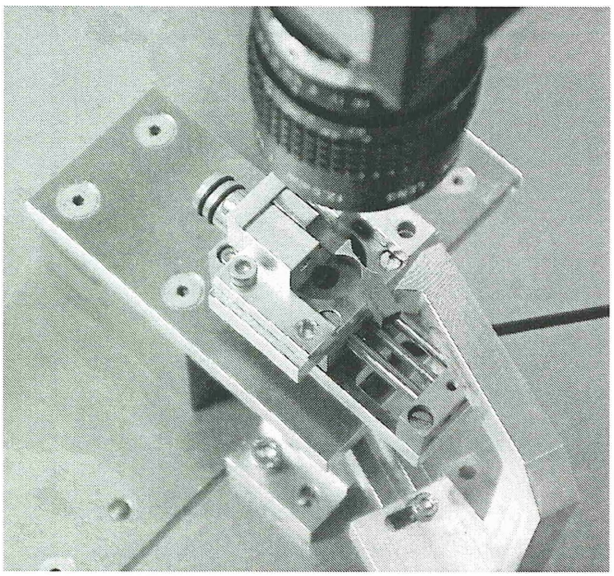

Figure 6. Experimental setup to measure the deflections and forces / moments of flexure hinges

Thereby, two different joint types were examined. The notch flexure hinge according to fig. 1, left and beam flexure hinge according to fig. 1, right. It permits larger angle deflections, because the deformation extends over the entire length l_M, but has also a larger movement of it's center of rotation.
(notch hinge: $l_1 = 25$ mm, $R = 6$ mm, $l_2 = 12$ mm, $t = 0.38$ mm, $h = 5$ mm, $b = 5$ mm)
(beam hinge: $l_1 = 19$ mm, $l_M = 12$ mm, $l_2 = 6$ mm, $t = 0.38$ mm, $h = 5$ mm, $b = 5$ mm)
The results of measurement compared to the calculated ones are shown in the diagrams 7 and 8. Generally the deviations for the z_B coordinate are smaller (differences less than 2%) than for the x_B coordinates, which are on average about 4%. Above all, this is due to the fact that for the x_B-coordinate only the deflections are measured. These are then added to the distance to the constraint. In z-direction the deflections are identical with the z_B-coordinate, thus it is measured absolutely. The deviations Δr from an ideal rotational joint during a deflection of $\phi_B = 20°$ are $\Delta r = 80\,\mu m$ at the notch hinge and $\Delta r = 0.35$mm at the beam hinge.

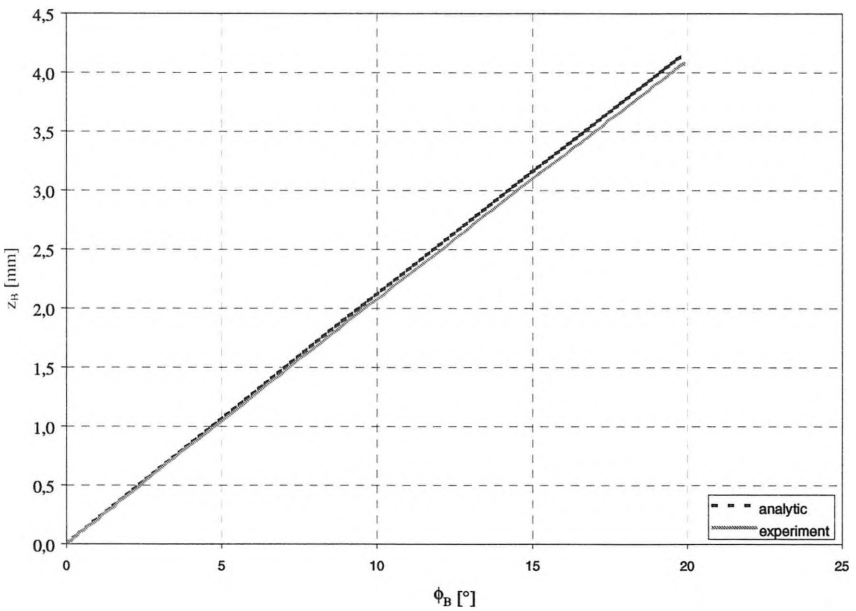

Figure 7. Measured and analytical computed deflections of a flexure hinge in z-direction

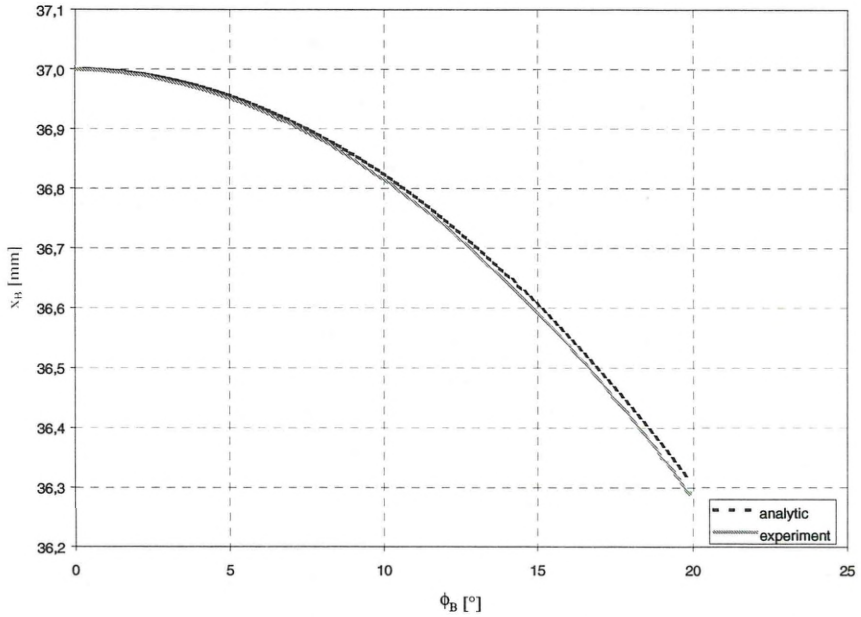

Figure 8. Measured and analytical computed deflections of a flexure hinge in x-direction

The movements of the instantaneous centers of rotation are seen in diagram 9. It is remarkable that the center of rotation of both hinges is not in the notching focal point (x = 25 mm) at the beginning, but it is displaced toward the constraint. Thereby, the larger the radius R or the length l_M is selected, the larger the displacement. With a long narrow cantilever beam with a constant cross section the center of rotation is about 1/3 length away from the constraint. In the case of the notch hinge the movement of the center of rotation is about 0.2 mm in both coordinates. In the case of the beam hinge, it is 0.14 mm in x-direction and 0.7 mm z-direction, in each case at an angle of rotation of $\phi_B = 20°$.

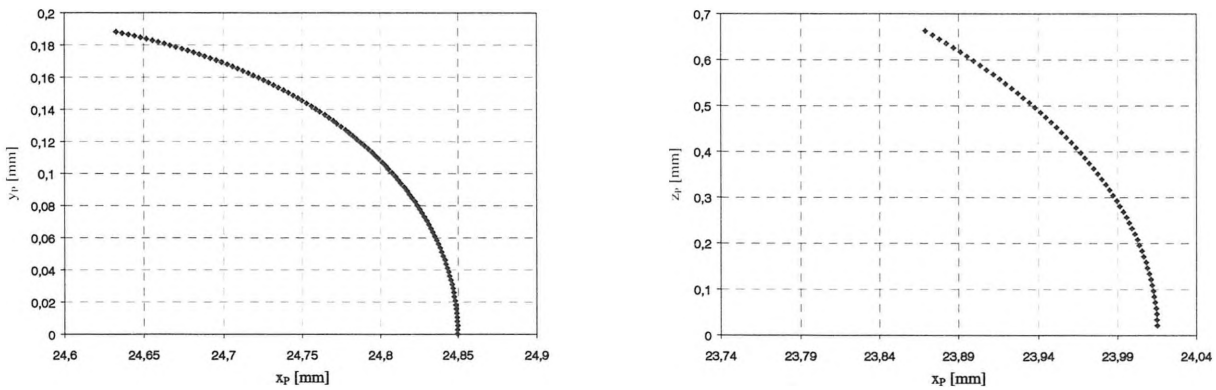

Figure 9. Movements of the center of rotation of a flexure notch hinge (left) and a flexure beam hinge (right), x_P and z_P are the coordinates of the fixed centroide

3. INTEGRATION OF FLEXURE HINGES IN A ROBOT FOR MICROASSEMBLY

Pseudo-elastic flexure notch hinges have been incorporated into a three (+1) degree-of-freedom parallel robot (fig. 10, micabo©)[13, 14]. The robot allows movement in x-, y-direction and a rotation about the z-axis. An additional lift table allows movements in z-direction as well. The robot is driven by piezo electric slip-stick actuators with a smallest step size of 5 nm and has incremental encoders with a resolution of 0.1 µm. The workspace is about 30x30 mm² with an angle of rotation of ±40°. Normally a gripper and a camera for visual control are integrated in the platform.

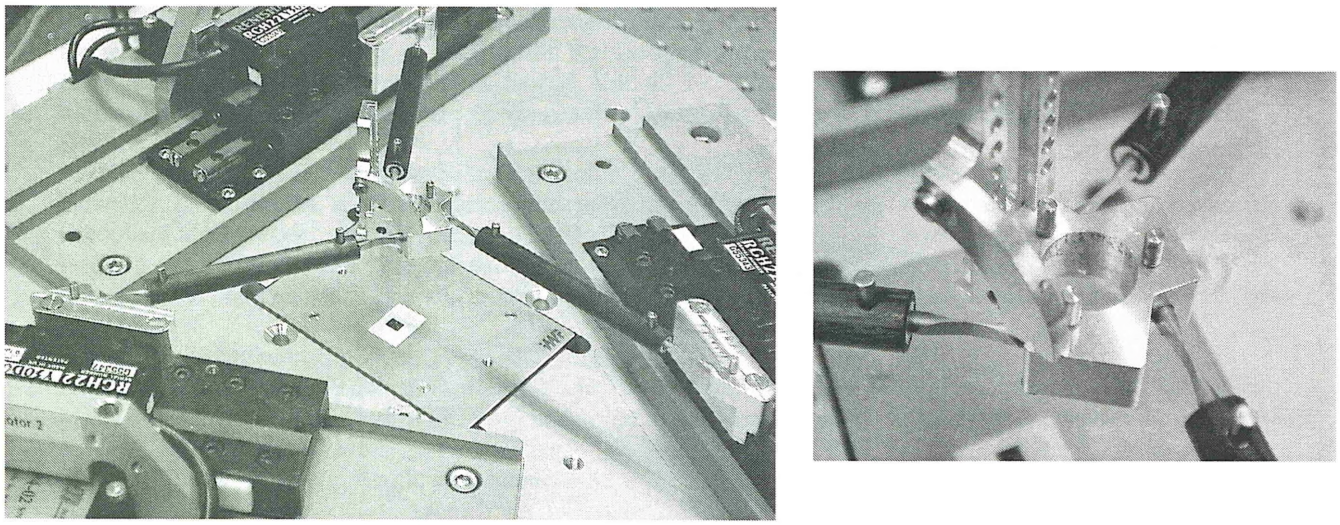

Figure 10. Parallel robot (micabo[c]) with integrated pseudo-elastic flexure notch hinges

Measurements with an earlier model of this robot led to a repeatability of 5µm without flexure hinges and a repeatability about 3µm with integrated flexure hinges. In this model flexure hinges made of CuAlNi single crystal alloy, with elastic strains up to 18%, are integrated. The radius R is 15 mm and the thinnest height t is 0.1 mm, which allows greater angular deflections. With no additional rotation of the platform the same workspace of 30x30 mm² could be used with the compliant mechanism. A rotation of 10° reduces the work space because of the strongly increasing angular deflections of the hinges. At a platform rotation of 10° the work space reduces to 30x12 mm², with an assumed maximal angular deflection of 20° with the hinges.

In order to investigate the influence of the kinematic deviations of the flexure hinges a simulation of the compliant mechanism is made in ANSYS. For a desired position and orientation of the tool center point (x_{TCP}, y_{TCP}, φ_{TCP}) the displacements q_i of the drives are computed via the model of the inverse kinematics.[15,16] These known values q_i are then used as constraints for certain nodes representing the drives in the FEM-model (fig. 11).

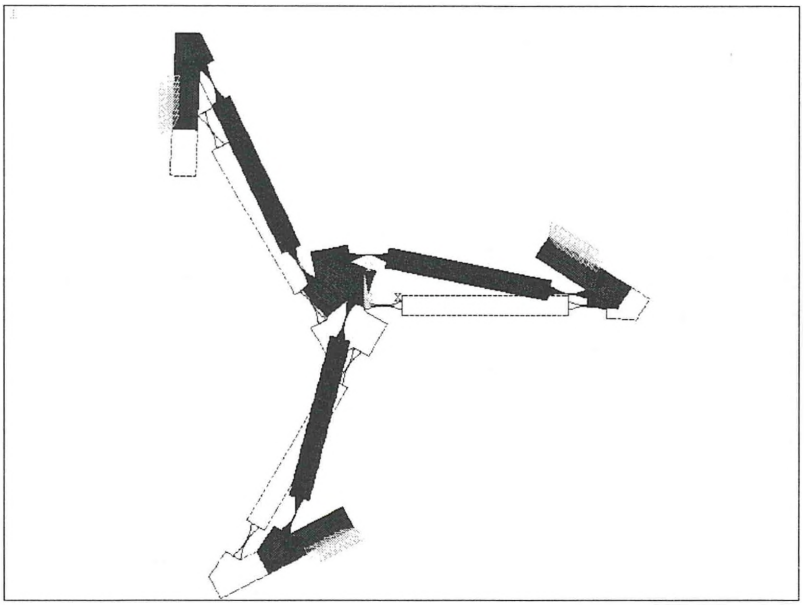

Figure 11. Deformation of the FEM-model of the compliant mechanism using the displacements q_i as constraints

In figure 12 the deviation Δr of the compliant mechanism computed with FEM and the kinematic model of the parallel structure with conventional joints are shown. Δr is the amount of the differences between the two tool center points, TCP_{FEM} and $TCP_{kin.\ model}$.

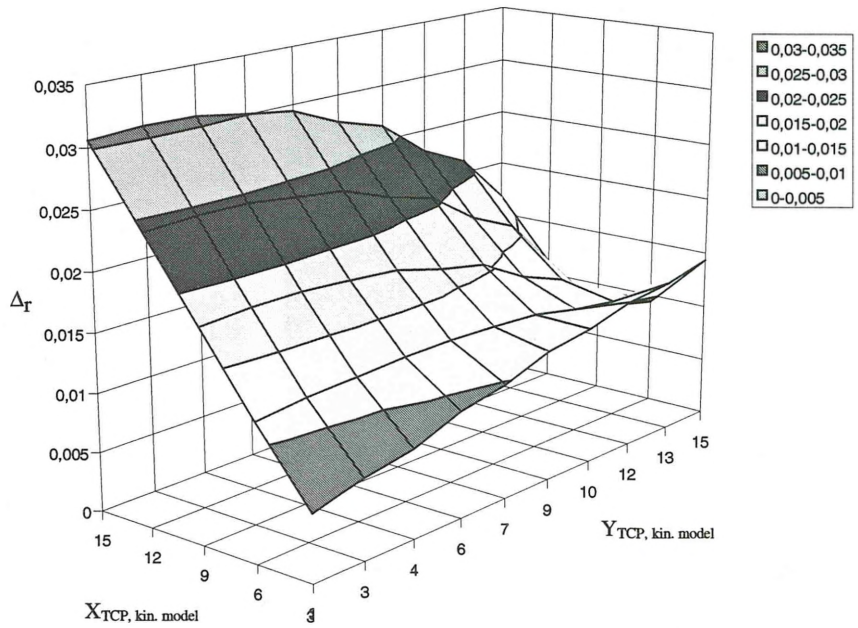

Figure 12. Deviation Δr of the compliant mechanism and the kinematic model of the parallel structure with conventional joints

The maximum deviation is about 31µm at $x_{TCP} = 15$ mm and $y_{TCP} = 4$ mm. Neither a general tendency nor a functional relation between the height of deviation and the position of the TCP can be determined. For certain positions the deviations due to the flexure hinges seem to compensate each other. This even results in a decrease of the center point deviation while x and y are increasing.

To increase the absolute accuracy of the compliant mechanism the deviations Δr have to be compensated via the robot control. One possible way to do this is to integrate the deviations of the flexure hinges compared to ideal rotational joints into the kinematic model of the structure. Therefore, the kinematic model of the flexure hinges shown in chapter 3 can be used. The new kinematic model of the structure will have variable kinematic parameters depending on the position of the tool center point. The advantage of this method is that it can be used for various parallel structures, if the kinematic model is known. This is far more efficient than computing the deviations of every single structure with FEM simulations.

4. CONCLUSIONS

A kinematic model describing the different kinematic behavior of flexure hinges in comparison to ideal rotational joints has been derived. This kinematic model is necessary if flexure hinges are integrated into parallel robots. With that the deviations of the flexure hinges can be included in the kinematic model of the structure. This will lead to a compensation of the deviations due to flexure hinges and will thereby maintain the absolute positioning accuracy of the parallel robot.

ACKNOWLEDGEMENTS

The authors gratefully acknowledge the financial support by the German Science Foundation (DFG HE 1890/ 11-1).

REFERENCES

1. Speich, J.E., Goldfarb, M., "A Three Degree-of-Freedom Flexure-Based Manipulator for High Resolution Spatial Micromanipulation", *Proceedings of SPIE Microrobotics and Micromanipulation*, Sulzman, A., Nelson, B. J., Vol. **3519**, p. 82-92, SPIE, Boston, 1998
2. Ryu, J.W., Gweon, D., Moon, K.S., "Optimal design of a flexure hinge based XYθ wafer stage", Precision Engineering, Vol. **21**, No. 1, p. 18-28, 1997
3. Pernette, E., Henein, S., Magnani, I., Clavel, R., "Design of parallel robots in microrobotics", Robotica, Vol. **15**, S. 417-420, 1997

4. Paros, J. and Weisbord, L., "How to Design Flexure Hinges", Machine Design, Vol. **37**, No. 27, pp. 151-156, 1965
5. Horie, M., Nozaki, T., Ikegami, K., Kobayashi, F., "Design Systems of Superelastic Hinges and its Application to Micromanipulators", JSME International Journal, Vol. **40**, No. 2, p. 323-328, 1997
6. Mertmann, M., NiTi-Formgedächtnislegierungen für Aktoren der Greifertechnik, Ph.D. thesis, Fortschr.-Berichte VDI Reihe 5, Nr. **469**, 1997
7. ANSYS User's Manual, Vol. **1** Procedures, Swanson Analysis Systems, Inc., 1994
8. Howell, L.L. and Midha, A., "Parametric Deflection Approximations for End-Loaded, Large-Deflection Beams in Compliant Mechanisms", ASME Journal of Mechanical Design, Vol. **116**, No. 1, pp. 156-165, 1995
9. Filonenko-Boroditsch, M.M., *Festigkeitslehre*, Band I+II, VEB Verlag Technik, Berlin, 1952
10. Pittschellis, R., Mechanische Miniaturgreifer mit Formgedächtnisantrieb, Ph.D. thesis, Fortschr.-Berichte VDI Reihe 2, Nr. **714**, 1998
11. Wuest, W., "Blattfedergelenke für Meßgeräte", Feinwerktechnik, Jg. 54, H. 7, 1950
12. Hesselbach, J., Ritter, R., Thoben, R., Reich, C., Pokar, G., "Visual Control and Calibration of Parallel Robots for Micro Assembly", *Proceedings of SPIE Microrobotics and Micromanipulation*, Sulzman, A., Nelson, B. J., Vol. **3519**, p. 50-61, SPIE, Boston, 1998
13. Thoben, R., Parallelroboter für die automatisierte Mikromontage, Ph.D. thesis, Fortschr.-Berichte VDI Reihe 8, Nr. **758**, 1999
14. Hesselbach, J., Pokar, G., "A class of new robots for micro assembly", Production Engineering, Vol. **VII/1**, p. 113-117, 2000
15. Alizade, R.I., Tagiyev, N.R., Duffy, J., "A forward and reverse displacement analysis of a 6-DOF in-parallel manipulator", Mechanism and Machine Theory, Vol. **29**, p. 115-124, 1994
16. Kerle, H., "Parallelroboter in der Handhabungstechnik – Bauformen, Berechnungsverfahren, Einsatzgebiete, VDI-Berichte, Nr. **1111**, p. 201-227, 1994